

# Ongoing evolution of submarine canyon rockwalls; examples from the Whittard Canyon, Celtic Margin (NE Atlantic)

Gareth D.O. Carter<sup>a\*</sup>, Veerle A.I. Huvenne<sup>b</sup>, Jennifer A. Gales<sup>c</sup>, Claudio Lo Iacono<sup>b</sup>, Leigh Marsh<sup>b,d</sup>, Audrey Ougier-Simonin<sup>e</sup>, Katleen Robert<sup>b</sup>, and Russell B. Wynn<sup>b</sup>

<sup>a</sup> British Geological Survey, The Lyell Centre, Research Avenue South, Edinburgh, EH14 4AP, UK

<sup>b</sup> Marine Geoscience, National Oceanography Centre, European Way, Southampton, SO14 3ZH, UK

<sup>c</sup> University of Plymouth, School of Biological and Marine Sciences, Drake Circus, Plymouth, PL4 8AA, UK

<sup>d</sup> Ocean and Earth Science, University of Southampton, Waterfront Campus, Southampton, SO14 3ZH, UK

<sup>e</sup> British Geological Survey, Environmental Science Centre, Nicker Hill, Keyworth, Nottingham, NG12 5GG, UK

\* Corresponding author: [gcarter@bgs.ac.uk](mailto:gcarter@bgs.ac.uk), +44 131 6500 373.

## ABSTRACT

During the CODEMAP 2015 research expedition to the Whittard Canyon, Celtic Margin (NE Atlantic), a Remotely Operated Vehicle (ROV) gathered High Definition (HD) video footage of the canyon rockwalls at depths of approx. 412 to 4184 mbsl. This dataset was supplemented by predominantly carbonate rock samples collected during the dives, which were subsequently tested for key physical property characteristics in a geotechnical laboratory. The high-resolution video footage revealed small-scale rockwall slope processes that would not have been visible if shipboard geophysical equipment was solely relied upon during the survey. Of particular interest was the apparent spalling failure of mudstone and chalk rockwalls, with fresh superficial “flaking” scars and an absence of sessile fauna possibly suggesting relatively recent mass-wasting activity. Extensive talus slopes, often consisting of coarse gravel, cobble and occasionally boulder-sized clasts, were observed at the foot of slopes impacted by spalling failures; this debris was rarely colonised by biological

60  
61  
62 32 communities, which could be an indicator of frequent rockfall events. Bio-erosion was also  
63  
64 33 noted on many of the walls prone to this form of rock slope failure (RSF). As in subaerial  
65  
66 34 equivalents, internal fracture networks appear to control the prevalence of RSF and the  
67  
68 35 geometries of blocks, often resulting in cubic and tabular blocks (0.2-1.0 m scale) of bedrock  
69  
70 36 toppling or sliding out of the cliff face. Tensile strength parameters of carbonate rock  
71  
72 37 samples were determined and these may affect the mass wasting processes observed within  
73  
74 38 the canyon. It was found that carbonate samples which appeared to have a higher mud  
75  
76 39 content, and reduced porosity, produced significantly higher tensile strength values. It is  
77  
78 40 proposed that these stronger, “muddy” carbonate units form the overhanging ledges that often  
79  
80 41 provide an ideal setting for sessile species, such as *Acesta excavata* clams, to colonise  
81  
82 42 whereas the weaker “pure” carbonate units are more easily eroded and therefore form the  
83  
84 43 undercutting, receding sections of the rockwall.

85  
86 44 By combining the ROV observations, basic discontinuity assessments (estimation of  
87  
88 45 fracture orientations) and laboratory testing results, an understanding of the geomechanical  
89  
90 46 properties of the bedrock can be obtained and linked with past and ongoing rock slope  
91  
92 47 processes within the Whittard Canyon. These conclusions will have a wider implication for  
93  
94 48 ongoing geomechanical processes within submarine canyons on a global scale.  
95  
96  
97  
98  
99

100 50 **Keywords:** submarine canyons, bedrock erosion, bioerosion, canyon rockwalls, Celtic  
101  
102  
103 51 Margin, NE Atlantic, Whittard Canyon, Remotely Operated Vehicle  
104  
105  
106

## 107 53 1. INTRODUCTION

108  
109 54 Submarine canyons comprise dynamic environments in which physical and biological  
110  
111 55 processes are constantly altering the slope morphology. The continuous transportation of  
112  
113 56 unconsolidated sediments downslope, and occasionally upslope, by local hydrodynamic  
114  
115  
116  
117  
118

119  
120  
121 57 forces has been well-documented within submarine canyons (e.g. Cunningham *et al.*, 2005;  
122  
123 58 Puig *et al.*, 2014). Large-scale mass wasting processes and sedimentological down-canyon  
124  
125 59 events such as turbidity currents are known to transport huge volumes of sediment through  
126  
127  
128 60 canyon systems (e.g. Sultan *et al.*, 2007; Lo Iacono *et al.*, 2011; Stewart *et al.*, 2014; Sumner  
129  
130 61 *et al.*, 2014; Talling, 2014).

132 62 However, there are only limited examples of studies that have investigated the effects  
133  
134 63 of bedrock processes on the morphology of submarine canyons. Despite submarine canyons  
135  
136 64 providing an obvious subaqueous setting where steep, often subvertical or overhanging,  
137  
138 65 bedrock terraces and cliffs are exposed at the seabed, very little research has been devoted to  
139  
140 66 the study of small-scale present-day bedrock erosional processes within these environments  
141  
142 67 and the subsequent consequences for ongoing canyon slope evolution. One example is the  
143  
144 68 study by Micallef *et al* (2012) which presented evidence of deep-seated mass wasting of  
145  
146 69 bedrock slopes within submarine canyons along the active tectonic margin of the Cook Strait,  
147  
148 70 New Zealand. While Micallef *et al* (2012) provided excellent detail on large-scale bedrock  
149  
150 71 landslides, including areas and volumes associated with slope failure events, small-scale  
151  
152 72 bedrock erosional processes and their implications for canyon slope evolution were not  
153  
154 73 discussed.

157 74 Chaytor *et al* (2016) did present evidence of small-scale bedrock failures within the  
158  
159 75 canyons of the U.S. Atlantic Continental Margin, and linked these processes with structural  
160  
161 76 controls within the bedrock units. However, the geomechanical properties of the different  
162  
163 77 lithological units were not investigated in detail, and the influence of engineering  
164  
165 78 characteristics (e.g. strength or porosity) upon bedrock slope erosion were not expanded upon  
166  
167 79 with quantitative data. McHugh *et al* (1993) provide a detailed study on the role of  
168  
169 80 diagenesis in the exfoliation of carbonate rocks within submarine canyons of the U.S.  
170  
171 81 Atlantic Continental Margin (offshore New Jersey). Visual observations of bedrock erosion,  
172  
173  
174  
175  
176  
177

178  
179  
180 82 associated with joint network propagation due to diagenetic transformation, were linked with  
181  
182 83 data collected by thin-section, scanning electron microscope/energy dispersive x-ray  
183  
184 84 (SEM/EDX) analyses. However, as with Chaytor *et al* (2016), geomechanical properties  
185  
186 85 were not investigated using geotechnical testing methods.  
187  
188

189 86 Previous studies from similar geological settings (e.g. Paull *et al* (1990a) focusing on  
190  
191 87 subvertical to vertical limestone cliffs of the Florida Escarpment) have highlighted evidence  
192  
193 88 of ongoing rock slope collapse. This suggests that the present-day slope profile of many  
194  
195 89 subaqueous bedrock terraces and cliffs may have been altered over time by modern erosional  
196  
197 90 processes.  
198

199 91 External factors can also contribute to the erosion of canyon slopes, with bioerosion  
200  
201 92 linked to benthic faunal communities being one source. A study by Dillon and Zimmerman  
202  
203 93 (1970) in two New England submarine canyons identified outcrops of sandstone, siltstone  
204  
205 94 and semi-consolidated mud that were riddled with burrows measuring up to 50 cm in  
206  
207 95 diameter, which were often occupied by crustaceans such as crabs. Bioerosion of this nature  
208  
209 96 has been noted in other U.S. submarine canyon systems (e.g. Warne *et al.*, 1978; Valentine  
210  
211 97 *et al.*, 1980).  
212  
213

214 98 Large-scale slope failures, such as those described by Micallef *et al* (2012), and  
215  
216 99 downslope sediment transfer processes (e.g. turbidity currents), as detailed by Sumner *et al*  
217  
218 100 (2014), are known to transfer sediments from upper canyon realms down towards the canyon  
219  
220 101 thalweg. However, what has not been well-documented to-date is the influence that small-  
221  
222 102 scale bedrock erosional processes can have upon canyon dynamics in relation to inducing  
223  
224 103 alterations to the geomorphology. In addition, when discussing mass transfer processes and  
225  
226 104 sedimentary budgets within submarine canyons (e.g. Puig *et al.*, 2003), bedrock erosional  
227  
228 105 processes have frequently been overlooked as a source of seafloor material within canyon  
229  
230 106 systems.  
231  
232  
233  
234  
235  
236

237  
238  
239 107 Many questions remain unanswered in relation to these erosional mechanisms; what  
240  
241 108 processes are contributing to bedrock erosion in submarine canyons? What role do the  
242  
243 109 geomechanical properties of different lithologies play in promoting ongoing slope erosion?  
244  
245 110 To what extent do benthic faunal communities influence the morphology of submarine slopes  
246  
247 111 and cliffs, including acting as a catalyst for slope erosion within canyon environments as  
248  
249 112 suggested by several authors (e.g. Rowe, 1974; Hecker, 1982)?  
250  
251

252 113 Here we provide detailed video evidence collected during multiple Remotely  
253  
254 114 Operated Vehicle (ROV) dives, highlighting small-scale present-day processes acting upon  
255  
256 115 bedrock slopes within the Whittard Canyon, Celtic Margin. Measurement of the physical  
257  
258 116 properties of rock samples collected from the canyon walls provide quantitative data, which  
259  
260 117 are used to investigate the impact of bedrock structures and lithology on slope stability. The  
261  
262 118 implications of these results on slope morphology and benthic habitats are discussed in the  
263  
264 119 context of the Whittard Canyon, and more widely in terms of subaqueous rockwalls on a  
265  
266 120 global scale.  
267  
268  
269 121

## 271 122 **2. GEOLOGICAL SETTING**

272  
273 123 The Whittard Canyon is a large dendritic canyon system extending from the shelf  
274  
275 124 edge (approximately 200 m below sea level (mbsl)) to the base of the continental slope at  
276  
277 125 approximately 4500 mbsl. It forms one of the most westerly of a number of submarine  
278  
279 126 canyon complexes located along the passive Celtic Margin (NE Atlantic), approximately 300  
280  
281 127 km SSW of the Republic of Ireland (Figure 1). The continental slope has an average gradient  
282  
283 128 of 8° in the vicinity of the Whittard Canyon, although it varies greatly across the Celtic  
284  
285 129 Margin due to multiple gully and canyon incisions (Amaro *et al.*, 2016). Towards the Goban  
286  
287 130 Spur Margin, which bounds the western extent of the Whittard Canyon complex, the  
288  
289 131 continental slope becomes more laterally continuous with an absence of slope incisions.  
290  
291  
292  
293  
294  
295

296  
297  
298 **FIGURE 1 – FULL PAGE (SEPARATE FILE, CAPTION AT END OF**  
299  
300  
301 **MANUSCRIPT)**

302  
303 134 Laterally, this abrupt change in slope morphology is heavily influenced by changes in  
304  
305 135 the underlying geological structure along the margin. However, the boundary between  
306  
307 136 continental and oceanic crust consistently controls the base of the slope throughout the  
308  
309 137 region, at approximately 4500 mbsl (Evans, 1990). The canyon itself was incised through  
310  
311 138 retrogressive mass wasting of the slope and headwall, instigated during the Pliocene –  
312  
313 139 Pleistocene (Amaro *et al.*, 2016). Although it has previously been noted that there is very  
314  
315 140 little or no evidence of present-day incision of the main axial channel (e.g. Stewart *et al.*,  
316  
317 141 2014; Amaro *et al.*, 2016), the evidence presented in this paper will demonstrate that the  
318  
319 142 major bedrock units that form canyon rockwalls are in no way inert and erosional processes  
320  
321 143 are ongoing.

322  
323  
324 144 The Early Cretaceous rifting episode of the North Atlantic resulted in the fault-block  
325  
326 145 topography upon which the Celtic Margin formed. These rotated fault-blocks are thought to  
327  
328 146 have influenced the profile of the lower slope, however the present day bathymetry of the  
329  
330 147 upper slope is the result of erosional processes (e.g. slumping and sediment density currents)  
331  
332 148 acting against the continued advancement of the shelf edge by sediment deposition (Evans,  
333  
334 149 1990).

335  
336 150 The post-rifting stratigraphy comprises Cretaceous chalk, Paleogene limestones and  
337  
338 151 mudstones, and Neogene calcareous clays, calcilutites (Jones Formation) and calcarenites  
339  
340 152 (Cockburn Formation), capped by Pliocene to Pleistocene sediments of the Little Sole  
341  
342 153 Formation (Evans & Hughes, 1984; Evans, 1990; Stewart *et al.*, 2014). No borehole logs  
343  
344 154 were available for the area of the shelf that immediately surrounds the canyon; however,  
345  
346 155 British Geological Survey (BGS) and Deep Sea Drilling Project (DSDP) cores provide a  
347  
348 156 general overview of the stratigraphy for the wider continental shelf and slope (Figure 1  
349  
350  
351  
352  
353  
354

355  
356  
357 157 (inset)). The Cretaceous chalks logged in BGS borehole +49-009/42 (Figure 2a), located  
358  
359 158 approximately 118 km NE (shelfward) of the canyon head, are described as being white to  
360  
361 159 pale grey, soft to firm, granular and glauconitic in places, and fossiliferous. Sporadic flint  
362  
363 160 nodules are also noted. Elsewhere, DSDP cores (Figure 2b) record carbonaceous and marly  
364  
365 161 nannofossil chalks of Cretaceous age (Montadert *et al.*, 1979). Paleogene soft clays, firm to  
366  
367 162 hard (and glauconitic in parts) limestone and fine-grained carbonaceous sandstone are present  
368  
369 163 in BGS borehole +49-009/42, overlain by Neogene clays that are calcareous, glauconitic,  
370  
371 164 carbonaceous and fossiliferous in nature. The DSDP borehole logs reveal siliceous  
372  
373 165 mudstones, silicified limestones, marly nannofossil chalks and nannofossil ooze of Paleogene  
374  
375 166 age, overlain by Neogene nannofossil chalks and oozes, siliceous mudstones, capped by  
376  
377 167 Pleistocene calcareous muds and nannofossil oozes (Montadert *et al.*, 1979). While these  
378  
379 168 borehole locations are not immediately adjacent to the Whittard Canyon, the formations  
380  
381 169 logged in these cores present a stratigraphic framework for the wider Celtic Margin into  
382  
383 170 which the canyon is incised.  
384  
385  
386

387 171 The oceanographic conditions of the Celtic Margin are characterized by high-energy  
388  
389 172 hydrodynamics, and tidal currents of up to  $0.9 \text{ m s}^{-1}$  have been recorded to the southeast of  
390  
391 173 the Whittard Canyon (around La Chapelle Bank), although these decrease to  $0.2 \text{ m s}^{-1}$  to the  
392  
393 174 northwest around the Goban Spur (Stewart *et al.*, 2014). These large tidal currents are  
394  
395 175 associated with equally large internal tides, guided through the major limbs of the canyon by  
396  
397 176 the seafloor topography (Aslam *et al.*, 2017). Near-bottom current velocities are intensified  
398  
399 177 along the canyon floor, highlighting the influence of canyon topography, and can lead to high  
400  
401 178 concentrations of suspended particles (Aslam *et al.*, 2017; Hall *et al.*, 2017). Along the Celtic  
402  
403 179 Margin, the strengthening of bottom current velocities affects sediment erosion at depths of  
404  
405 180 400 – 500 m (Cunningham *et al.*, 2005). The hydrodynamics across the wider region are  
406  
407 181 known to transport sediments from the near shore, across the shelf and down the margin slope  
408  
409  
410  
411  
412  
413

414  
415  
416 182 (Stewart *et al.*, 2014). Towards the head of the Whittard Canyon, a series of large (up to 55  
417  
418 183 m high and 200 km long) linear sand ridges were formed between 10 – 20 cal ka, orientated  
419  
420 184 perpendicular to the shelf break (Scourse *et al.*, 2009). These sand ridges, and sandwave  
421  
422 185 fields shelfward of the canyon head, provide a source of sediment for modern transport  
423  
424 186 processes. Present-day down-slope gravity flows have also been noted to transport sediment  
425  
426 187 from the shelf edge down through the canyon (Amaro *et al.*, 2016), and contour currents are  
427  
428 188 responsible for along-slope transport of sediments across the Celtic Margin (Stewart *et al.*,  
429  
430 189 2014).  
431  
432

433 190 **FIGURE 2 – HALF PAGE (SEPARATE FILE, CAPTION AT END OF**  
434  
435 191 **MANUSCRIPT)**  
436  
437  
438 192

439  
440 193 **3. DATA AND METHODS**

441  
442 194 Rock samples and video images from the canyon walls were collected over a four-  
443  
444 195 week period during Expedition JC125 as part of the CODEMAP 2015 project (COMplex  
445  
446 196 Deep-sea Ecosystems: Mapping habitat heterogeneity As Proxy for biodiversity), funded by  
447  
448 197 the European Research Council (Grant No. 258482), onboard the *RRS James Cook*.  
449

450 198 Videos were collected over 17 dives, from depths of approx. 412 to 4184 mbsl, by the  
451  
452 199 Natural Environment Research Council's (NERC) *Isis* ROV, a science-class system that has a  
453  
454 200 maximum dive depth of 6500 mbsl (Huvenne *et al.*, 2016). The *Isis* ROV uses two different  
455  
456 201 navigation systems; a Sonardyne Ultra-Short Base Line system (USBL) and a Doppler  
457  
458 202 Velocity Log (DVL) dead-reckoning (Huvenne *et al.*, 2016). The video imagery was  
459  
460 203 collected using three optically corrected High-Definition (HD) cameras which were mounted  
461  
462 204 to the front of the ROV; one camera was used primarily for piloting the vehicle, another  
463  
464 205 camera was operated (pan, tilt and zoom functions) by members of the science party during  
465  
466  
467  
468  
469  
470  
471  
472



473  
474  
475 206 dive operations, and the third camera was kept on a fixed angle and zoom level (Huvenne *et*  
476  
477 207 *al.*, 2016).

479 208 In addition to the video footage, the ROV collected seven carbonate rock samples  
480  
481 (representative of the lithology at each particular dive depth) which were suitable for strength  
482 209 testing using point load test (PLT) and uniaxial compressive strength (UCS) methods (ASTM  
483  
484 210 Standards D5731–5795, 2001, and D2938-95, 2002, respectively). Due to the volume and  
485  
486 211 standard dimensions of material required for UCS testing, only one rock sample recovered by  
487  
488 212 the ROV was suitable for this method. The samples had average dimensions of 218.7 mm x  
489  
490 213 147.6 mm x 65.9 mm, and were acquired from the base of terraces and cliffs that exhibited  
491  
492 214 erosional scars (Figure 1). The highly brittle nature of the mudstones prevented the ROV  
493  
494 215 from obtaining a sample of this lithology. A single sample was acquired from a bioturbated  
495  
496 216 muddy terrace within the thalweg of the western branch; this sample was classified as a soil  
497  
498 217 sample in engineering property terms. All tests were conducted at room temperature,  
499  
500 218 following the ISRM suggested methodologies (Franklin, 1985; Fairhurst and Hudson, 1999;  
501  
502 219 Ulusay and Hudson, 2007) and ASTM standards (ASTM Standards: D4318-10, 2000;  
503  
504 220 D5731–5795, 2001; D2938-95, 2002; D3148-02, 2002; D4543-04, 2004) taking into account  
505  
506 221 the limited material available. The carbonate rock specimens were tested both oven dried and  
507  
508 222 wet using distilled water.  
509  
510 223

513 224 **FIGURE 3 – FULL PAGE (SEPARATE FILE, CAPTION AT END OF**  
514  
515 225 **MANUSCRIPT)**

## 519 227 **4. RESULTS**

### 522 228 **4.1 BEDROCK SLOPE PROCESSES**

524 229 Evidence of active erosion was observed at various depths and across a variety of  
525  
526 230 different bedrock lithologies. The most prevalent of these processes was the widespread  
527  
528  
529  
530  
531

532  
533  
534  
535  
536  
537  
538  
539  
540  
541  
542  
543  
544  
545  
546  
547  
548  
549  
550  
551  
552  
553  
554  
555  
556  
557  
558  
559  
560  
561  
562  
563  
564  
565  
566  
567  
568  
569  
570  
571  
572  
573  
574  
575  
576  
577  
578  
579  
580  
581  
582  
583  
584  
585  
586  
587  
588  
589  
590

231 exfoliation or spalling failure of vertical to subvertical cliff and terraced surfaces (Figure 3a  
& b). The most significant erosion was noted in areas of apparently weak mudstone,  
232 although occurrences of exfoliation were also noted on carbonate and chalk surfaces (Figure  
233 3c). Typically, flakes or cobbles of mudstone were noted to have produced significant  
234 accumulations in the form of talus deposits at the base of terraces and cliffs. The exposed  
235 face above these talus slopes exhibits patches of fresh, light grey, scar surfaces often adjacent  
236 to brown, weathered surfaces unaffected by recent spalling (Figure 3b). The detritus forming  
237 the talus slopes is predominantly angular in shape, and composed of generally cobble to  
238 occasionally boulder sized clasts, with the surfaces of these slopes being notably devoid of  
239 any established benthic communities (Figure 3d). On the carbonate (predominantly chalk)  
240 units, shallow exfoliation of the exposed surface was visible in the form of flaked patches of  
241 fresh, bright white scars (devoid of benthic fauna) adjoining areas of beige, weathered  
242 surfaces that were often colonized by sessile fauna (Figure 3c).

244 Active retreat of terraced mudstone slopes through spalling erosion was noted on 11  
245 separate occasions over the course of the 17 ROV dives (Figure 3a & b). Additionally, the  
246 undermining of basal sections of mudstone terraces through localized spalling failure and  
247 bioerosion was observed (Figure 3b).

248 In addition to spalling failure, evidence of block failure was observed in mudstone  
249 and carbonate units. In all lithologies, discontinuity orientation (bedding and joint sets) was  
250 noted to be a controlling factor, creating planes of weakness within the rock mass resulting in  
251 repeated rock slope failure. Cubic blocks of mudstone, measuring up to approx. 1.0 m in  
252 length, occur on talus slopes beneath cliffs exhibiting fresh block failure scars. These blocks  
253 occasionally displayed multiple internal fractures along parallel planes; the orientation of  
254 these fractures mirrors the failure planes that bound the toppled blocks, suggesting consistent  
255 structural weaknesses exist within the bedrock terrace above (Figure 3e). In carbonate units,

591  
592  
593 256 perpendicular vertical to subvertical joint sets (orientations estimated using the ROV  
594  
595 257 navigation data), result in small (approx. 0.2-0.5 m) wedge block failures where bedding  
596  
597 258 planes dipped out of the face of the rockwall (Figure 3f). Failure along these exposed  
598  
599 259 laterally continuous bedrock ledges resulted in a “saw-tooth” profile and associated  $\leq 0.5$  m  
600  
601 260 diameter diamond-shaped detachment blocks around the base of the ledge.  
602  
603

604 261 The mode of failure appears to be predominantly lithologically controlled, as spalling  
605  
606 262 and block failures were noted at various water depths (i.e. differing pressure and temperature  
607  
608 263 gradients) and in areas of varying hydrodynamic conditions (e.g. current velocities).  
609

610 264 Examples of canyon wall erosion within mudstone units were chiefly noted at water depths of  
611  
612 265 between 850 – 1050 mbsl, with block failures of carbonate ledges noted at approx. 750 mbsl  
613  
614 266 and spalling/exfoliation of chalk cliff faces noted between approx. 2,000 – 3,500 mbsl. It is  
615  
616 267 likely that these failure mechanisms mainly reflect the physical properties of the stratigraphic  
617  
618 268 units exposed in the canyon rock wall at these depths, and external factors (e.g. water  
619  
620 269 temperature) play a reduced role in rock slope erosion.  
621  
622

623 270 Although large-scale rock slope failures (RSF) were not the main focus of this study,  
624  
625 271 boulder fields were observed, particularly towards the thalweg of the canyon. These typically  
626  
627 272 consisted of subrounded to subangular boulders (often  $>1.0$  m in axial length) of mixed  
628  
629 273 lithologies, embedded within the canyon floor sediments suggesting sufficient time has  
630  
631 274 passed for this buildup of sediments to occur post-failure (Figure 4a & b). As many of these  
632  
633 275 large clasts were in contact with adjacent boulders (as opposed to overlying), and embedded  
634  
635 276 to similar depths within canyon floor sediments, this would suggest that the failure of each  
636  
637 277 block occurred simultaneously or within a short timeframe. However, as no rock avalanche  
638  
639 278 scars were observed in the canyon walls above, it is not possible to conclusively state whether  
640  
641 279 these boulders were deposited during one catastrophic failure event or are the result of  
642  
643 280 continued (and possibly ongoing) individual toppling failure episodes.  
644  
645  
646  
647  
648  
649

650  
651  
652 281  
653  
654 282 **FIGURE 4 – HALF PAGE (SEPARATE FILE, CAPTION AT END OF**  
655  
656 **MANUSCRIPT)**  
657 283  
658  
659 284

660  
661 285 **4.2 LABORATORY TEST RESULTS**  
662

663 286 The carbonate rock samples could be roughly divided into two groups based on  
664  
665 287 appearance; fine to medium grained, white to yellowish grey on weathered surfaces, with  
666  
667 288 open, smooth, irregular voids and no evidence of secondary carbonate precipitation. These  
668  
669 289 samples were possibly oolitic and also fragmentary on weathered surfaces. Carbonate  
670  
671 290 samples from the second group were fine to medium grained, very light grey to dark  
672  
673 291 yellowish orange on weathered surfaces, massive with no obvious void spaces and no internal  
674  
675 292 structure, and fragmentary on weathered surfaces. Samples from this group were noted to be  
676  
677 293 muddier than those of the white carbonate group, in both appearance and texture. The  
678  
679 294 unconsolidated sediment sample (soil in engineering terms) was identified as a silty clay  
680  
681 295 through particle size analysis (Figure 5a).

682  
683  
684 296 The strength experiments revealed two distinct groups of carbonate rock: the muddy  
685  
686 297 carbonates group which has a lower porosity and a higher strength than the pure carbonates  
687  
688 298 group by a factor of about three and two to eight, respectively (Table 1 and Figure 5b). The  
689  
690 299 muddy carbonates are classified as high to very high strength rocks while the pure carbonates  
691  
692 300 are low to medium strength (Figure 5c) (Broch & Franklin, 1972). No clear effect on the  
693  
694 301 mechanical strength could be related to the saturation condition (Figure 5b).

695  
696  
697 302 The plasticity plot (Figure 5d) shows the unconsolidated silty clay to be highly plastic.  
698  
699 303

700  
701 304 **TABLE 1 – FULL PAGE (FOOT OF MANUSCRIPT WITH CAPTION)**  
702  
703 305  
704  
705  
706  
707  
708

709  
710  
711 306 **FIGURE 5 – HALF PAGE (SEPARATE FILE, CAPTION AT END OF**  
712  
713 307 **MANUSCRIPT)**  
714  
715  
716 308

717  
718 309 **4.3 INFLUENCE OF BENTHOS ON CANYON SLOPE STABILITY**

719  
720 310 Prominent features of the surveyed mudstone terraces included shallow borings (up to  
721  
722 311 approx. 2 cm diameter) and approx. 5-10 cm diameter burrows caused by benthic organisms,  
723  
724 312 often clustered into highly concentrated areas (Figure 4c & d).  
725

726 313 Spalling and exfoliation is prevalent where terrace surfaces have been extensively  
727  
728 314 bored and it was noted that fresh surfaces exposed following spalling failure were devoid of  
729  
730 315 borings whereas adjacent, weathered surfaces were heavily bioeroded (Figure 4c).  
731

732  
733 316 In addition to the shallow borings, rows of adjacent burrows were noted along the  
734  
735 317 base of mudstone cliffs and terraces (up to 10 cm in diameter). These often appeared to  
736  
737 318 penetrate into the strata to depths exceeding 10 cm, although it was not possible to ascertain  
738  
739 319 maximum penetration depths within the terrace. Burrows were often situated within 20-50  
740  
741 320 cm of each other, resulting in sections of the base of terraces being gradually undermined.  
742

743 321 Bioindicators of mass wasting were present across the canyon walls. These included  
744  
745 322 sections of carbonate ledges and walls where the absence of coral and other sessile fauna may  
746  
747 323 potentially highlight relatively recent spalling and block failures. Similar indicators were  
748  
749 324 visible on slopes completely dominated by coral communities, where failure of poorly  
750  
751 325 consolidated mudstone resulted in visible scars devoid of any benthic colonies.  
752

753  
754 326  
755  
756 327 **5. DISCUSSION**

757  
758 328 Observations and data gathered during the CODEMAP 2015 research cruise to the  
759  
760 329 Whittard Canyon clearly illustrate the influence that both lithology and biological activity  
761  
762 330 may have upon rates of bedrock erosion over relatively short timescales.  
763  
764  
765  
766  
767

768  
769  
770 **5.1 LITHOLOGICAL CONTROLS ON ROCK SLOPE EROSION**  
771

772 332 Multiple instances of spalling failure were noted, which appeared to have the greatest  
773  
774 333 influence on cliffs and terraces composed of mudstone units. This differs from other  
775  
776 334 geographical locations where spalling failure has been documented in similar marine  
777  
778 335 environments; for instance, this process has been observed in submarine canyons along the  
780  
781 336 U.S. Atlantic Continental Margin by Chaytor *et al* (2016), where it mainly affected  
782  
783 337 carbonate-rich and chalk lithologies, and not mudstone terraces as is the case in the Whittard  
784  
785 338 Canyon. Observations also suggest that spalling failure and erosion of mudstone terraces  
786  
787 339 may influence the stability of overlying stratigraphic units. Where active mudstone terrace  
788  
789 340 retreat is occurring beneath more competent bedrock units (e.g. carbonates), and where  
790  
791 341 undermining along the base of terraced slopes is taking place, there is often an increase in  
792  
793 342 internal stresses within the overlying formation; this is known to result in rockfalls and  
794  
795 343 toppling failures onshore (Highland and Bobrowsky, 2008), and is likely to also be true for  
796  
797 344 the cases observed within the Whittard Canyon.

799  
800 345 Block failures are controlled by inherent structural weaknesses within the bedrock  
801  
802 346 units, clearly visible in the form of perpendicular joint sets. Blocks of both mud and  
803  
804 347 carbonate lithologies were observed at the base of bedrock terraces where bedding planes  
805  
806 348 were noted to dip out of the cliff face. These blocks exhibited similar geometries (size and  
807  
808 349 orientation of surfaces), suggesting that regularly spaced joint sets are a common feature of  
809  
810 350 the stratigraphic units forming the bedrock terraces.

812  
813 351 Onshore, rock strength is known to be critical for the stability of rock slopes with  
814  
815 352 outward dipping bedding planes, as the roughness of the joint provides frictional resistance  
816  
817 353 against failure (Selby, 1982). As the geotechnical results revealed that the pure carbonate  
818  
819 354 units were of weak to medium strength, the shearing of asperities along these joints due to  
820  
821 355 slope loading or increased stresses associated with bioerosion may result in the loss of  
822

827  
828  
829  
830  
831  
832  
833  
834  
835  
836  
837  
838  
839  
840  
841  
842  
843  
844  
845  
846  
847  
848  
849  
850  
851  
852  
853  
854  
855  
856  
857  
858  
859  
860  
861  
862  
863  
864  
865  
866  
867  
868  
869  
870  
871  
872  
873  
874  
875  
876  
877  
878  
879  
880  
881  
882  
883  
884  
885

356 frictional resistance and subsequently block failure. Rock slope failures from steep carbonate  
357 cliffs are not unknown; Paull *et al* (1990a) reported on fresh rock surfaces across the Florida  
358 Escarpment which they linked with episodic collapse of the limestone terraces, highlighting  
359 that subaqueous carbonate cliffs are still subjected to active erosion and modification at this  
360 present time.

361 In carbonate lithologies, dissolution along joints, caused by the expulsion of  
362 formation fluids, has been linked with initiating block failure by reducing the frictional  
363 resistance along discontinuities in submerged rock slopes (McHugh *et al.*, 1993). Chemical  
364 weathering of joints through spring sapping has even been proposed as a model for canyon  
365 formation (e.g. Robb, 1984; Paull *et al.*, 1990b), illustrating the erosive potential of fluid  
366 expulsion and migration along major joints and faults. This form of biochemical weathering  
367 is challenging to identify at individual discontinuity resolution using ROV footage, however  
368 aperture widths of >1 cm were noted within carbonate outcrops and karstic features that are  
369 typically indicative of dissolution and fluid flow were observed in chalk units.

370 In addition, the geotechnical testing results show that the strength of the carbonate  
371 units varies considerably depending on the apparent fine particle content; as the mud content  
372 appears to increase (based on visual descriptions of the samples), pore spaces are reduced and  
373 the carbonate unit becomes stronger. Shallow exfoliation and spalling of carbonate units may  
374 be more prevalent across these weaker, purer carbonate lithologies where the internal shear  
375 strength can be exceeded by external forces such as loading and drag from attached sessile  
376 fauna. Block failure scars were numerous in areas of visibly porous, weak carbonate ledges  
377 that were often densely populated by large communities of the clam *Acesta excavata* and  
378 associated cold-water corals, adding additional stress through gravitational and drag forcing  
379 which acts upon the intrinsically weak lithology.

886  
887  
888  
889 380 It is difficult to determine why spalling and exfoliation erosion is so prevalent across  
890  
891 381 the lithological units of the Whittard Canyon. The McHugh *et al* (1993) study into the role of  
892  
893 382 diagenesis in exfoliation of carbonate units within submarine canyons of the U.S. Atlantic  
894  
895 383 Continental Margin links the fracturing of bedrock with the volume reduction of silica-rich  
896  
897 384 chalks, driven by fluid expulsion during progressive burial. As overburden is removed  
898  
899 385 during canyon incision and mass wasting processes, the diagenetically formed fractures  
900  
901 386 expand and exfoliation can occur (McHugh *et al.*, 1993). As failure is induced by loss of  
902  
903 387 support, stress release continues and erosion in the form of spalling and block failures can  
904  
905 388 occur on the exposed, fractured rock surface (McHugh *et al.*, 1993). In this way, a continual  
906  
907 389 cycle of terrace and cliff face erosion is maintained, and provides a plausible model for the  
908  
909 390 exfoliation of carbonate units within the Whittard Canyon.

911  
912 391 Due to the highly plastic nature (atberberg limits of samples JC125\_060\_#1; Figure 1)  
913  
914 392 and the high clay content of the sampled soil, shrink-swell behavior was considered as a  
915  
916 393 factor for spalling of mudstone surfaces within the study area. However, the marine  
917  
918 394 environment under which these sediments were deposited and incised should prevent such  
919  
920 395 phenomenon as the clay should not shrink/swell due to it being in a fully saturated state. The  
921  
922 396 potential for shrink-swell to occur would remain if these clays are bearing some non-saline  
923  
924 397 water and this is exchanged for salt water. However, even if this were to occur, the effect on  
925  
926 398 the volume would likely remain very small. For these reasons, shrink-swell has been  
927  
928 399 discounted as being a major controlling factor on the observed spalling failure of mudstone  
929  
930 400 terraces/cliffs.

933 401 The single clay sample (JC125\_060\_#1) represents an unconsolidated sediment  
934  
935 402 terrace as opposed to a bedrock terrace, and therefore it does not give an accurate  
936  
937 403 representation of the weak mudstone terraces observed elsewhere in the canyon. It is  
938  
939 404 pertinent that the ROV failed to acquire a consolidated mudstone sample from the observed  
940  
941  
942  
943  
944



945  
946  
947 405 bedrock terraces, due to the brittle nature of the available material, as this indicates the  
948  
949 406 general weak state of the mudstone units surveyed.

## 951 407 **5.2 EXTERNAL INFLUENCES ON BEDROCK EROSION**

952  
953 408 Other factors that may influence bedrock slope erosion include the local  
954  
955  
956 409 hydrodynamics, whereby current velocities exert increased shear stresses upon the base and  
957  
958 410 surfaces of vertical walls, promoting undercutting processes and shallow quarrying of the  
959  
960 411 exposed outcrops (Mitchell *et al.*, 2013; Mitchell, 2014). However, as the studies by Mitchell  
961  
962 412 *et al* (2013) and Mitchell (2014) highlight, bed shear stresses typically need to exceed 100 Pa  
963  
964 413 before quarrying and plucking of jointed bedrock can occur and would therefore be unlikely  
965  
966 414 to take place in the Whittard Canyon if relying exclusively on mean current velocities alone.  
967  
968 415 Mitchell (2006; 2014) did observe that sediment flows may well produce the bed shear  
969  
970 416 stresses required to initiate plucking and quarrying of bedrock within a canyon system, and  
971  
972 417 turbidity currents are known to occur within the Whittard Canyon system (e.g. Cunningham  
973  
974 418 *et al.*, 2005).

975  
976 419 Burrowing and boring faunal communities also play an active role in spalling failure  
977  
978 420 within the Whittard canyon; it is likely that clusters of multiple borings are responsible for  
979  
980 421 creating a plane of weakness subparallel to the exposed surface, controlled by the depth at  
981  
982 422 which the organisms have excavated. This would result in a reduction in the rock mass  
983  
984 423 strength, leading to failure (Hecker, 1982). Chaytor *et al* (2016) noted the same phenomenon  
985  
986 424 in carbonate-rich lithologies within canyons along the U.S. Atlantic Continental Margin  
987  
988 425 where the failure depth of surface material appeared to be controlled by the depth of  
989  
990 426 bioerosion. Burrows and borings of a similar nature have been reported in exposed mudstone  
991  
992 427 units in the Monterey Canyon, California, leading to bioerosion of the bedrock slope (Paull *et*  
993  
994 428 *al.*, 2005). Burrows along the base of mudstone terraces, similar to those identified by Dillon  
995  
996  
997  
998  
999  
1000  
1001  
1002  
1003

1004  
1005  
1006  
1007  
1008  
1009  
1010  
1011  
1012  
1013  
1014  
1015  
1016  
1017  
1018  
1019  
1020  
1021  
1022  
1023  
1024  
1025  
1026  
1027  
1028  
1029  
1030  
1031  
1032  
1033  
1034  
1035  
1036  
1037  
1038  
1039  
1040  
1041  
1042  
1043  
1044  
1045  
1046  
1047  
1048  
1049  
1050  
1051  
1052  
1053  
1054  
1055  
1056  
1057  
1058  
1059  
1060  
1061  
1062

429 and Zimmerman (1970), also effectively undermine the material above, leading to a decrease  
430 in the internal strength within the rock mass, which in turn would exacerbate terrace collapse.

431 Analysis of the video footage suggests that sessile fauna may also influence bedrock  
432 erosion within the Whittard Canyon. In areas of block failures and shallow exfoliation  
433 surfaces associated with the carbonate units, additional loading may be applied to the  
434 terrace/cliff face through the erosive actions of sessile organisms. This can lead to an  
435 increase in drag and gravitational forces (Hecker, 1982), and could be especially pertinent  
436 within areas of the significantly weaker, pure carbonates. Sample L1, which produced very  
437 low to medium strength point load results ( $I_{s50}$  0.051 – 0.460), was noted to be heavily  
438 encrusted with coral and other sessile organisms upon recovery from the base of the rock  
439 slope.

440 The bedrock erosion mechanisms observed during expedition JC125 have  
441 implications that extend beyond the area of the Whittard Canyon. While it is widely  
442 documented that slope processes around the Celtic Margin include active erosion of margin  
443 slopes, to-date studies have had a singular focus on unconsolidated sediment processes (e.g.  
444 Cunningham *et al.*, 2005; Leynaud *et al.*, 2009). Evidence of spalling and block failure  
445 across multiple exposed lithologies demonstrates ongoing erosion of the stratigraphic bedrock  
446 framework upon which the NE Atlantic Continental Margin sediments are draped. Given that  
447 the vast majority of the strata recovered in boreholes around the shelf and slope (e.g. Figure  
448 2) are of carbonate or mud/clay composition, a significant proportion of the exposed bedrock  
449 terraces/cliffs along the Celtic Margin is likely to be susceptible to the aforementioned  
450 mechanisms of failure. This would suggest that the exposed bedrock cliffs and terraces are in  
451 fact active and not inert features of the margin slopes.

452 Chaytor *et al* (2016) used the presence (and absence) of slow growing corals and  
453 sponges to demonstrate long-term stability of canyon rockwalls and relative timings of rock

1063  
1064  
1065  
1066  
1067  
1068  
1069  
1070  
1071  
1072  
1073  
1074  
1075  
1076  
1077  
1078  
1079  
1080  
1081  
1082  
1083  
1084  
1085  
1086  
1087  
1088  
1089  
1090  
1091  
1092  
1093  
1094  
1095  
1096  
1097  
1098  
1099  
1100  
1101  
1102  
1103  
1104  
1105  
1106  
1107  
1108  
1109  
1110  
1111  
1112  
1113  
1114  
1115  
1116  
1117  
1118  
1119  
1120  
1121

454 slope failures across canyons of the U.S. Atlantic Continental Margin. While no baseline  
455 data is available to ascertain rates of erosion, the observed failure surfaces exhibited clear  
456 fresh, and therefore relatively recent, scars and slopes were often devoid of benthic  
457 communities implying recolonization had probably not taken place yet. Many erosional  
458 scars, which were fresh in appearance with no benthic faunal communities attached, were  
459 surrounded by well-established coral communities suggesting relatively recent failure of the  
460 slope surface. In relation to the wider Celtic Margin and Whittard Canyon system, the large-  
461 scale sediment slumps that have been documented are singular events that are likely to be  
462 relatively infrequent when compared with the bedrock erosional processes.

463         The spalling of bedrock terraces and structurally-controlled block failures, coupled  
464 with the geotechnical laboratory results, suggest that morphological alteration of the  
465 rockwalls that underpin the Whittard Canyon is currently ongoing. In addition,  
466 morphological modification of rock slopes through bioerosion was noted across several ROV  
467 dives. A limited number of studies have noted these erosional processes in submarine  
468 canyons across both active and passive margins elsewhere; Chaytor *et al* (2016) highlighted  
469 the presence of similar spalling failures associated with clusters of borings in carbonate units  
470 forming submarine canyon rockwalls across the U.S. Atlantic Continental Margin, and Paull  
471 *et al* (2005) reported on notches, small caves and burrows penetrating and modifying  
472 mudstone slopes that had become exposed through the mass wasting of overlying sediments  
473 within the Monterey Canyon, California. This would suggest that these processes have wide  
474 implications for the stability of submarine canyon rockwalls on a global scale. Furthermore,  
475 research undertaken by Paull *et al* (1990a) on the Florida Escarpment also highlights that  
476 these erosional processes influence the morphology of subaqueous bedrock slopes in different  
477 geological settings and are therefore not only limited to rockwalls within submarine canyons.

1122  
1123  
1124 478 Further work to better define the contribution of these small-scale processes on  
1125  
1126 479 canyon evolution, which have been underestimated until the present day is still required,  
1127  
1128  
1129 480 especially in relation to the physical properties of bedrock units. In addition, further studies  
1130  
1131 481 on the influence of benthic fauna on the modification of rock slope morphology within  
1132  
1133 482 submarine canyons would be beneficial. At present, the role that rock slope erosion has upon  
1134  
1135 483 sediment transfer and quantitative budgets within submarine canyons has not been  
1136  
1137 484 determined, and this should also be investigated further.  
1138  
1139 485

## 1141 486 6. CONCLUSIONS

1142  
1143 487 ROV observations coupled with geotechnical laboratory measurements have allowed  
1144  
1145  
1146 488 for a detailed assessment of the Whittard Canyon rockwalls to be undertaken. The following  
1147  
1148 489 conclusions can be drawn; (1) Ongoing spalling erosion is prevalent throughout the canyon,  
1149  
1150 490 particularly affecting brittle mudstone units. This process results in the build-up of  
1151  
1152 491 substantial talus slopes at the base of eroding terraces, and may lead to the undermining of  
1153  
1154 492 more competent units above; (2) Block failures within carbonate units are controlled by the  
1155  
1156 493 orientation of discontinuity joint sets, in addition to intrinsic strength properties which appear  
1157  
1158 494 to be influenced by the fine mud content (and therefore the available pore space) of the  
1159  
1160 495 lithology and; (3) Benthic organisms have the potential to exacerbate slope erosion in several  
1161  
1162 496 ways, and evidence of ongoing bioerosion was observed across mudstone and carbonate  
1163  
1164 497 lithologies.

1165  
1166  
1167 498 Due to a lack of published data relating to submarine canyon rockwalls, it is  
1168  
1169 499 impossible to confirm that these erosional processes also occur at similar rates and with  
1170  
1171 500 similar results in submarine canyons worldwide. However, some of the processes described  
1172  
1173 501 above have been noted in canyons along the U.S. NW Atlantic Margin (Chaytor *et al.*, 2016)  
1174  
1175 502 and within the Monterey Canyon, California (Paull *et al.*, 2005). Our results highlight the  
1176  
1177  
1178  
1179  
1180

1181  
1182  
1183  
1184  
1185  
1186  
1187  
1188  
1189  
1190  
1191  
1192  
1193  
1194  
1195  
1196  
1197  
1198  
1199  
1200  
1201  
1202  
1203  
1204  
1205  
1206  
1207  
1208  
1209  
1210  
1211  
1212  
1213  
1214  
1215  
1216  
1217  
1218  
1219  
1220  
1221  
1222  
1223  
1224  
1225  
1226  
1227  
1228  
1229  
1230  
1231  
1232  
1233  
1234  
1235  
1236  
1237  
1238  
1239

503 requirement for further studies to assess the contribution of the observed processes in canyon  
504 evolutionary models and to better understand the interactive processes between benthic  
505 communities and mass failure within submarine canyons.

506

507 **ACKNOWLEDGEMENTS**

508 This work was made possible by the CODEMAP 2015 research expedition to the  
509 Whittard Canyon, Celtic Margin (funded by ERC Starting Grant 258482 and the NERC  
510 MAREMAP programme). A special thank you to all members of the CODEMAP 2015  
511 science team, and the captain and crew of the *RRS James Cook*. Gareth Carter publishes with  
512 permission of the Director of the British Geological Survey (Natural Environment Research  
513 Council). The authors would like to extend their sincerest gratitude to the reviewers  
514 (Katherine Maier, United States Geological Survey, and Neil Mitchell, University of  
515 Manchester, UK) and the Guest Editor (Pere Puig, Spanish National Research Council) for  
516 their hugely constructive and encouraging feedback and comments on this manuscript. The  
517 authors are also grateful to Emrys Phillips, British Geological Survey, for internal review of  
518 the manuscript before submission.

519

520 **REFERENCES**

521 Amaro, T., Huvenne, V. A. I., Allcock, A. L., Aslam, T., Davies, J. S., Danovaro, R.,  
522 De Stigter, H. C., Duineveld, G. C. A., Gambi, C., Gooday, A. J., Gunton, L. M., Hall, R.,  
523 Howell, K. L., Ingels, J., Kiriakoulakis, K., Kershaw, C. E., Lavaleye, M. S. S., Robert, K.,  
524 Stewart, H., Van Rooij, D., White, M. and Wilson, A.M. (2016). The Whittard Canyon – A  
525 case study of submarine canyon processes. *Progress in Oceanography*, 146, 38–57.

526 Aslam, T., Hall, R. A., & Dye, S. R. (2017). Internal tides in a dendritic submarine  
527 canyon. *Progress in Oceanography*.

- 1240  
1241  
1242 528           ASTM Standard D2938-95, 2002, Standard Test Method for Unconfined  
1243  
1244 529   Compressive Strength of Intact Rock Core Specimens: ASTM International, West  
1245  
1246   Conshohocken, PA, [www.astm.org](http://www.astm.org).  
1247 530  
1248  
1249 531           ASTM Standard D3148-02, 2002, Standard Test Method for Elastic Moduli of Intact  
1250  
1251 532   Rock Core Specimens in Uniaxial Compression: ASTM International, West Conshohocken,  
1252  
1253 533   PA, [www.astm.org](http://www.astm.org).  
1254  
1255 534           ASTM Standard D4318-10, 2000, Standard test methods for liquid limit, plastic limit,  
1256  
1257 535   and plasticity index of soils: ASTM International, West Conshohocken, PA, [www.astm.org](http://www.astm.org).  
1258  
1259 536           ASTM Standard D4543-04, 2004, Standard Practices for Preparing Rock Core  
1260  
1261 537   Specimens and Determining Dimensional and Shape Tolerances: ASTM International, West  
1262  
1263 538   Conshohocken, PA, [www.astm.org](http://www.astm.org).  
1264  
1265  
1266 539           ASTM Standard D5731–5795, 2001, Standard method for determination of the point  
1267  
1268 540   load strength index of rock: ASTM International, West Conshohocken, PA, [www.astm.org](http://www.astm.org).  
1269  
1270 541           Broch, E. and Franklin, J. A. (1972). The point-load strength test. *International*  
1271  
1272 542   *Journal of Rock Mechanics and Mining Sciences & Geomechanics Abstracts*, 9, 669–676.  
1273  
1274 543           Chaytor, J. D., Demopoulos, A. W. J., ten Brink, U. S., Baxter, C., Quattrini, A. M.  
1275  
1276 544   and Brothers, D. S. (2016). Assessment of Canyon Wall Failure Process from Multibeam  
1277  
1278 545   Bathymetry and Remotely Operated Vehicle (ROV) Observations, U.S. Atlantic Continental  
1279  
1280 546   Margin. In G. Lamarche, J. Mountjoy, S. Bull, T. Hubble, S. Krastel, E. Lane, A. Micallef, L.  
1281  
1282 547   Moscardelli, C. Mueller, I. Pecher, and S. Woelz (Eds.), *Submarine Mass Movements and*  
1283  
1284 548   *their Consequences*, 7<sup>th</sup> *International Symposium* (pp. 103–113). Switzerland, Springer  
1285  
1286 549   International Publishing.  
1287  
1288  
1289 550           Cunningham, M. J., Hodgson, S., Masson, D. G. and Parson, L. M. (2005). An  
1290  
1291 551   evaluation of along-and down-slope sediment transport processes between Goban Spur and  
1292  
1293 552   Brenot Spur on the Celtic Margin of the Bay of Biscay. *Sedimentary Geology*, 79(1), 99–116.  
1294  
1295  
1296  
1297  
1298

1299  
1300  
1301  
1302  
1303  
1304  
1305  
1306  
1307  
1308  
1309  
1310  
1311  
1312  
1313  
1314  
1315  
1316  
1317  
1318  
1319  
1320  
1321  
1322  
1323  
1324  
1325  
1326  
1327  
1328  
1329  
1330  
1331  
1332  
1333  
1334  
1335  
1336  
1337  
1338  
1339  
1340  
1341  
1342  
1343  
1344  
1345  
1346  
1347  
1348  
1349  
1350  
1351  
1352  
1353  
1354  
1355  
1356  
1357

553           Dillon, W. P. and Zimmerman, H. B. (1970). Erosion by biological activity in two  
554 New England submarine canyons. *Journal of Sedimentary Research*, 40(2), 542-547.

555           Evans, C. D. R. and Hughes, M. J. (1984). The Neogene succession of the South  
556 Western Approaches, Great Britain. *Journal of the Geological Society*, 141(2), 315–326.

557           Evans, C. D. R. (1990) *The geology of the western English Channel and its western*  
558 *approaches*. London, HMSO for the British Geological Survey, 93 p.

559           Fairhurst, C. E. and Hudson, J. A. (1999). Draft ISRM suggested method for the  
560 complete stress-strain curve for intact rock in uniaxial compression, ISRM suggested  
561 methods (SMs): second series. *International Journal of Rock Mechanics and Mining*  
562 *Sciences*, 36, 279–289.

563           Franklin, J. A. (1985). Suggested method for determining point load strength, ISRM  
564 suggested methods. *International Journal of Rock Mechanics and Mining Sciences &*  
565 *Geomechanics Abstracts*, 22, 51–60.

566           Hall, R. A., Aslam, T., & Huvenne, V. A. (2017). Partly standing internal tides in a  
567 dendritic submarine canyon observed by an ocean glider. *Deep Sea Research Part I:*  
568 *Oceanographic Research Papers*.

569           Hecker, B. (1982). Possible benthic fauna and slope instability relationships. In S.  
570 Saxov and J. K. Nieuwenhuis (Eds.), *Marine Slides and Other Mass Movements* (pp. 335–  
571 347). New York, Plenum.

572           Highland, L. and Bobrowsky, P. T. (2008). The landslide handbook: a guide to  
573 understanding landslides (p. 129). Reston, U.S. Geological Survey.

574           Huvenne, V. A. I., Wynn, R. B. and Gales, J. A. (2016). RRS James Cook Cruise 124-  
575 125-126. CODEMAP2015: Habitat mapping and ROV vibrocorer trials around Whittard  
576 Canyon and Haig Fras. National Oceanography Centre Open-File Report (Cruise Report No.  
577 36).

- 1358  
1359  
1360  
1361 578 Leynaud, D., Mienert, J. and Vanneste, M. (2009). Submarine mass movements on  
1362 579 glaciated and non-glaciated European continental margins: a review of triggering  
1363 580 mechanisms and preconditions to failure. *Marine and Petroleum Geology*, 26(5), p. 618–632.  
1364  
1365  
1366  
1367 581 Lo Iacono, C., Sulli, A., Agate, M., Lo Presti, V., Pepe, F. and Catalano, R. (2011).  
1368 582 Submarine canyon morphologies in the Gulf of Palermo (Southern Tyrrhenian Sea) and  
1370 583 possible implications for geo-hazard. *Marine Geophysical Research*, 32(1-2), 127–138,  
1371 584 doi:10.1007/s11001-011-9118-0.  
1372  
1373  
1374  
1375 585 McHugh, C. M., Ryan, W. B. and Schreiber, B. C. (1993). The role of diagenesis in  
1376 586 exfoliation of submarine canyons. *AAPG Bulletin*, 77(2), 145-172.  
1377  
1378  
1379 587 Micallef, A., Mountjoy, J. J., Canals, M. and Lastras, G. (2012). Deep-seated bedrock  
1380 588 landslides and submarine canyon evolution in an active tectonic margin: Cook Strait, New  
1381 589 Zealand. In Y. Yamada, K. Kawamura, K. Ikehara, Y. Ogawa, R. Urgeles, D. Mosher, J.  
1382 590 Chaytor, and M. Strasser (Eds.), *Submarine Mass Movements and their Consequences*, 5<sup>th</sup>  
1383 591 *International Symposium* (pp. 201–212). Netherlands, Springer.  
1384  
1385  
1386  
1387  
1388  
1389  
1390 592 Mitchell, N. C. (2006). Morphologies of knickpoints in submarine canyons.  
1391 593 *Geological Society of America Bulletin*, 118(5-6), 589-605.  
1392  
1393  
1394 594 Mitchell, N. C., Huthnance, J. M., Schmitt, T. and Todd, B. (2013). Threshold of  
1395 595 erosion of submarine bedrock landscapes by tidal currents. *Earth Surface Processes and*  
1396 596 *Landforms*, 38(6), 627-639.  
1397  
1398  
1399  
1400 597 Mitchell, N. C. (2014). Bedrock erosion by sedimentary flows in submarine canyons.  
1401 598 *Geosphere*, 10(5), 892-904.  
1402  
1403  
1404  
1405 599 Montadert, L., Roberts, D. G., Auffret, G. A., Bock, W. D., Dupeuble, P. A.,  
1406 600 Hailwood, E. A., Harrison, W. E., Kagami, H., Lumsden, D. N., Muller, C. M., Schnitker, D.,  
1407 601 Thompson, R. W., Thompson, T. L., Timofeev, P. P., and Mann, D. (1979). Deep Sea  
1408 602 Drilling Project (DSDP), Site 402/Hole 402A, doi:10.2973/dsdp.proc.48.105.1979.  
1409  
1410  
1411  
1412  
1413  
1414  
1415  
1416



1417  
1418  
1419  
1420  
1421  
1422  
1423  
1424  
1425  
1426  
1427  
1428  
1429  
1430  
1431  
1432  
1433  
1434  
1435  
1436  
1437  
1438  
1439  
1440  
1441  
1442  
1443  
1444  
1445  
1446  
1447  
1448  
1449  
1450  
1451  
1452  
1453  
1454  
1455  
1456  
1457  
1458  
1459  
1460  
1461  
1462  
1463  
1464  
1465  
1466  
1467  
1468  
1469  
1470  
1471  
1472  
1473  
1474  
1475

603 Paull, C. K., Freeman-Lynde, R., Bralower, T. J., Gardemal, J. M., Neumann, A. C.,  
604 D'Argenio, B. and Marsella, E. (1990a). Geology of the strata exposed on the Florida  
605 Escarpment. *Marine Geology*, 91(3), 177-194.

606 Paull, C. K., Spiess, F. N., Curray, J. R. and Twichell, D. C. (1990b). Origin of  
607 Florida Canyon and the role of spring sapping on the formation of submarine box canyons.  
608 *Geological Society of America Bulletin*, 102(4), 502-515.

609 Paull, C. K., Ussler, W., Greene, H. G., Barry, J. and Keaten, R. (2005). Bioerosion  
610 by chemosynthetic biological communities on Holocene submarine slide scars. *Geo-Marine*  
611 *Letters*, 25(1), 11-19.

612 Puig, P., Ogston, A. S., Mullenbach, B. L., Nittrouer, C. A., & Sternberg, R. W.  
613 (2003). Shelf-to-canyon sediment-transport processes on the Eel continental margin (northern  
614 California). *Marine Geology*, 193(1), 129-149.

615 Puig, P., Palanques, A., and Martín, J. (2014). Contemporary sediment-transport  
616 processes in submarine canyons. *Annual review of marine science*, 6, 53-77.

617 Robb, J. M. (1984). Spring sapping on the lower continental slope, offshore New  
618 Jersey. *Geology*, 12(5), 278-282.

619 Rowe, G. T. (1974). The effects of the benthic fauna on the physical properties of  
620 deep-sea sediments. In A. Inderbitzen (Ed.), *Deep-Sea Sediments: Physical and Mechanical*  
621 *Properties* (pp. 381–400). New York, Springer.

622 Scourse, J., Uehara, K., and Wainwright, A. (2009). Celtic Sea linear tidal sand  
623 ridges, the Irish Sea Ice Stream and the Fleuve Manche: palaeotidal modelling of a  
624 transitional passive margin depositional system. *Marine Geology*, 259(1), 102-111.

625 Selby, M. J. (1982). Controls on the stability and inclinations of hillslopes formed on  
626 hard rock. *Earth Surface Processes and Landforms*, 7(5), 449-467.

1476  
1477  
1478 627 Stewart, H. A., Davies, J. S., Guinan, J. and Howell, K. L. (2014). The Dangeard and  
1479  
1480 628 Explorer canyons, South Western Approaches UK: Geology, sedimentology and newly  
1481  
1482 629 discovered cold-water coral mini-mounds. *Deep Sea Research Part II: Topical Studies in*  
1483  
1484 630 *Oceanography*, 104, 230–244.  
1485  
1486  
1487 631 Sultan, N., Gaudin, M., Berne, S., Canals, M., Urgeles, R. and Lafuerza, S. (2007).  
1488  
1489 632 Analysis of slope failures in submarine canyon heads: an example from the Gulf of Lions.  
1490  
1491 633 *Journal of Geophysical Research: Earth Surface*, 112(F1), doi:10.1029/2005JF000408.  
1492  
1493 634 Sumner, E. J., Peakall, J., Dorrell, R. M., Parsons, D. R., Darby, S. E., Wynn, R. B.,  
1494  
1495 635 McPhail, S. D., Perrett, J., Webb, A., and White, D. (2014). Driven around the bend: Spatial  
1496  
1497 636 evolution and controls on the orientation of helical bend flow in a natural submarine gravity  
1498  
1499 637 current. *Journal of Geophysical Research: Oceans*, 119(2), 898-913.  
1500  
1501 638 Talling, P. J. (2014). On the triggers, resulting flow types and frequencies of  
1502  
1503 639 subaqueous sediment density flows in different settings. *Marine Geology*, 352, 155-182.  
1504  
1505 640 Ulusay, R. and Hudson, J. A. (2007). The complete ISRM suggested methods for rock  
1506  
1507 641 characterization, testing and monitoring: 1974-2006. In R. Ulusay and J. A. Hudson (Eds.),  
1508  
1509 642 *Commission on testing methods. International Society of Rock Mechanics. Compilation*  
1510  
1511 643 *arranged by ISRM Turkish National Group*. Turkey, Springer.  
1512  
1513 644 Valentine, P. C., Uzzmann, J. R. and Cooper, R. A. (1980). Geologic and biologic  
1514  
1515 645 observations in Oceanographer submarine canyon: descriptions of dives aboard the research  
1516  
1517 646 submersibles Alvin (1967, 1978) and Nekton Gamma (1974). *U.S. Geological Survey Open*  
1518  
1519 647 *File Report*, 80–76: 40 pp.  
1520  
1521 648 Warne, J. E., Slater, R. A. and Cooper, R. A. (1978). Bioerosion in submarine  
1522  
1523 649 canyons. In D. J. Stanley and G. Kelling (Eds.), *Sedimentation in submarine canyons, fans,*  
1524  
1525 650 *and trenches*. Stroudsburg, Pennsylvania, Dowden, Hutchinson and Ross, p. 65–70.  
1526  
1527  
1528  
1529 651  
1530  
1531  
1532  
1533  
1534

1535  
1536  
1537 652 **FIGURE AND TABLE CAPTIONS**  
1538  
1539 653  
1540

1541 654 **Figure 1:** Location of study area (red box) is inset, with locations of boreholes displayed (orange dot for BGS borehole  
1542 655 and yellow dots for DSDP boreholes). Main figure shows hillshaded bathymetric map of the Whittard Canyon gridded to  
1543 656 50 m overlying GEBCO data. Locations of rock samples and bedrock erosion observations are shown.

1544 657  
1545  
1546 658 **Figure 2:** (A) BGS borehole +49-009/42 (K.B. Kelly Bushing) and (B) DSDP borehole 402, illustrating regional stratigraphy  
1547 659 across the shelf and slope into which the Whittard Canyon is incised (adapted from Montadert *et al.*, 1979).

1548 660  
1549  
1550 661 **Figure 3:** (a) & (b) show spalling/exfoliation surfaces on mudstone terraces, resulting in cliffline retreat; (c) exfoliation on  
1551 662 a chalk cliff surface; (d) extensive accumulations of mudstone material at base of spalling terrace, forming a talus slope;  
1552 663 and (e) & (f) show structurally controlled block failures in mudstone and carbonate units respectively.

1553  
1554 664  
1555  
1556 665 **Figure 4:** (a) & (b) boulders of mixed lithologies embedded in canyon floor sediments; (c) shallow borings cover the  
1557 666 terrace surface to the left of the image, whereas the fresh, exfoliation surface is devoid of borings and; (d) larger borings  
1558 667 penetrating a weathered mudstone terrace.

1559 668  
1560  
1561 669 **Figure 5:** Summary of geotechnical results (a) grain size analysis of the unconsolidated sediment sample, showing it to be  
1562 670 a silty clay; (b) effective porosity vs strength (c) rock strength (Point Load Test & Unconfined Compressive Strength) of  
1563 671 pure carbonates and muddy carbonates (d) plasticity plot for silty clay sample.

1564 672  
1565  
1566 673 **Table 1:** Point Load Index (PLI) testing results, showing the difference in strength values between pure  
1567 674 and muddy carbonate samples.

1568  
1569 675  
1570  
1571  
1572  
1573  
1574  
1575  
1576  
1577  
1578  
1579  
1580  
1581  
1582  
1583  
1584  
1585  
1586  
1587  
1588  
1589  
1590  
1591  
1592  
1593

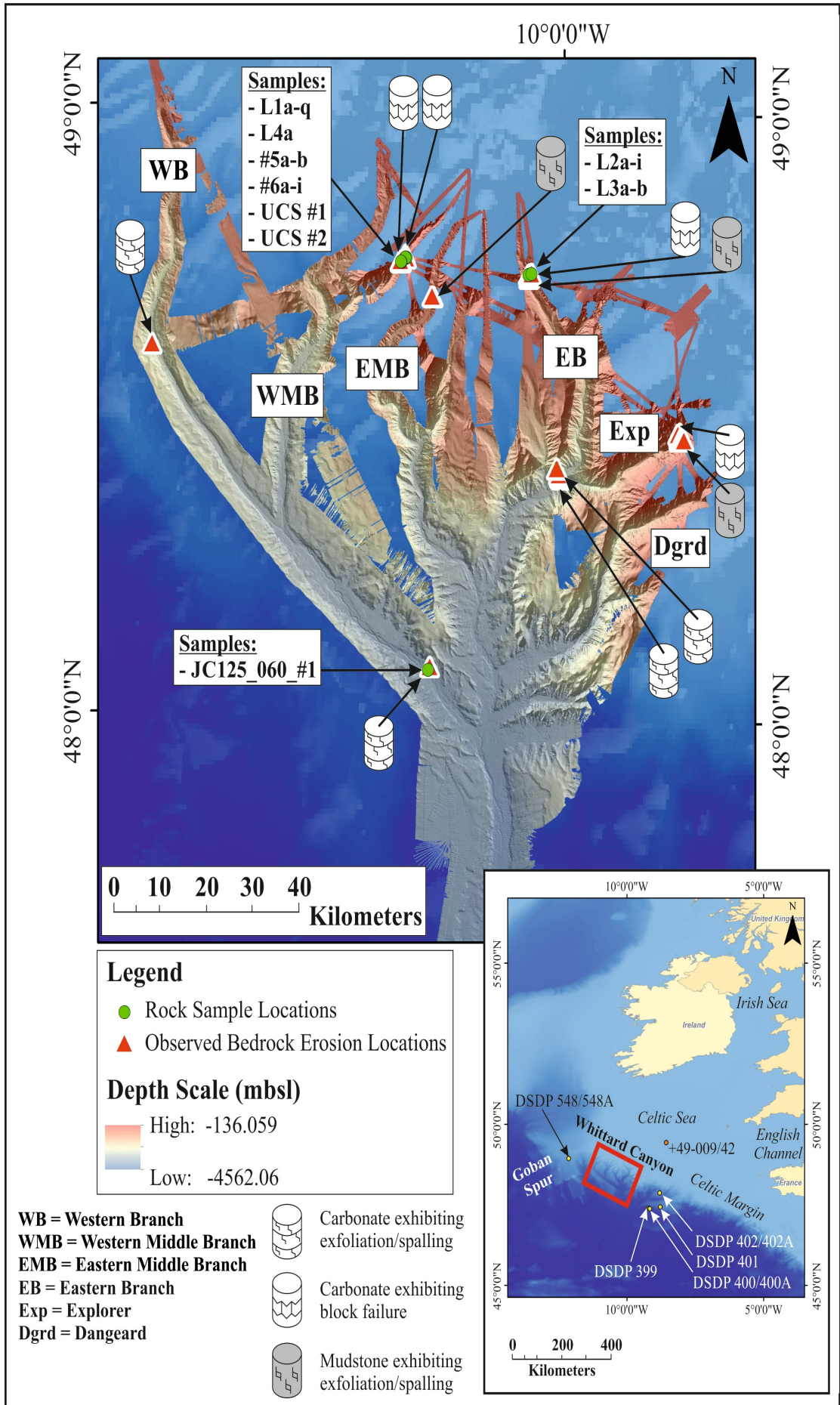
1594  
 1595  
 1596  
 1597  
 1598  
 1599  
 1600  
 1601  
 1602  
 1603  
 1604  
 1605  
 1606  
 1607  
 1608  
 1609  
 1610  
 1611  
 1612  
 1613  
 1614  
 1615  
 1616  
 1617  
 1618  
 1619  
 1620  
 1621  
 1622  
 1623  
 1624  
 1625  
 1626  
 1627  
 1628  
 1629  
 1630  
 1631  
 1632  
 1633  
 1634  
 1635  
 1636  
 1637  
 1638  
 1639  
 1640  
 1641  
 1642  
 1643  
 1644  
 1645  
 1646  
 1647  
 1648  
 1649  
 1650  
 1651  
 1652

Sample ID	Sample Type	Depth (mbsl)	Latitude	Longitude	IS <sub>50</sub>
L1a	pure carbonate	-736.30	48.759976	-10.458456	0.263
L1b	pure carbonate	-736.30	48.759976	-10.458456	0.252
L1c	pure carbonate	-736.30	48.759976	-10.458456	0.223
L1d	pure carbonate	-736.30	48.759976	-10.458456	0.280
L1e	pure carbonate	-736.30	48.759976	-10.458456	0.209
L1f	pure carbonate	-736.30	48.759976	-10.458456	0.401
L1g	pure carbonate	-736.30	48.759976	-10.458456	0.079
L1h	pure carbonate	-736.30	48.759976	-10.458456	0.120
L1i	pure carbonate	-736.30	48.759976	-10.458456	0.333
L1j	pure carbonate	-736.30	48.759976	-10.458456	0.460
L1k	pure carbonate	-736.30	48.759976	-10.458456	0.100
L1l	pure carbonate	-736.30	48.759976	-10.458456	0.088
L1m	pure carbonate	-736.30	48.759976	-10.458456	0.073
L1n	pure carbonate	-736.30	48.759976	-10.458456	0.080
L1o	pure carbonate	-736.30	48.759976	-10.458456	0.051
L1p	pure carbonate	-736.30	48.759976	-10.458456	0.135
L1q	pure carbonate	-736.30	48.759976	-10.458456	0.081
L2a	pure carbonate	-491.50	48.737467	-10.090386	0.263
L2b	pure carbonate	-491.50	48.737467	-10.090386	0.306
L2c	pure carbonate	-491.50	48.737467	-10.090386	0.212
L2d	pure carbonate	-491.50	48.737467	-10.090386	0.366
L2e	pure carbonate	-491.50	48.737467	-10.090386	0.268
L2f	pure carbonate	-491.50	48.737467	-10.090386	0.245
L2g	pure carbonate	-491.50	48.737467	-10.090386	0.282
L2h	pure carbonate	-491.50	48.737467	-10.090386	0.211
L2i	pure carbonate	-491.50	48.737467	-10.090386	0.163
L3a	pure carbonate	-874.00	48.735818	-10.099441	0.121
L3b	pure carbonate	-874.00	48.735818	-10.099441	0.338
L4a	pure carbonate	-760.30	48.760368	-10.461013	0.345
#5a	muddy carbonate	-838.00	48.753295	-10.472528	2.382
#5b	muddy carbonate	-838.00	48.753295	-10.472528	2.527
#6a	muddy carbonate	-841.00	48.753296	-10.472546	3.045
#6b	muddy carbonate	-841.00	48.753296	-10.472546	2.608
#6c	muddy carbonate	-841.00	48.753296	-10.472546	2.729
#6d	muddy carbonate	-841.00	48.753296	-10.472546	2.064
#6e	muddy carbonate	-841.00	48.753296	-10.472546	0.845
#6f	muddy carbonate	-841.00	48.753296	-10.472546	2.716
#6g	muddy carbonate	-841.00	48.753296	-10.472546	2.364
#6h	muddy carbonate	-841.00	48.753296	-10.472546	2.233
#6i	muddy carbonate	-841.00	48.753296	-10.472546	0.585

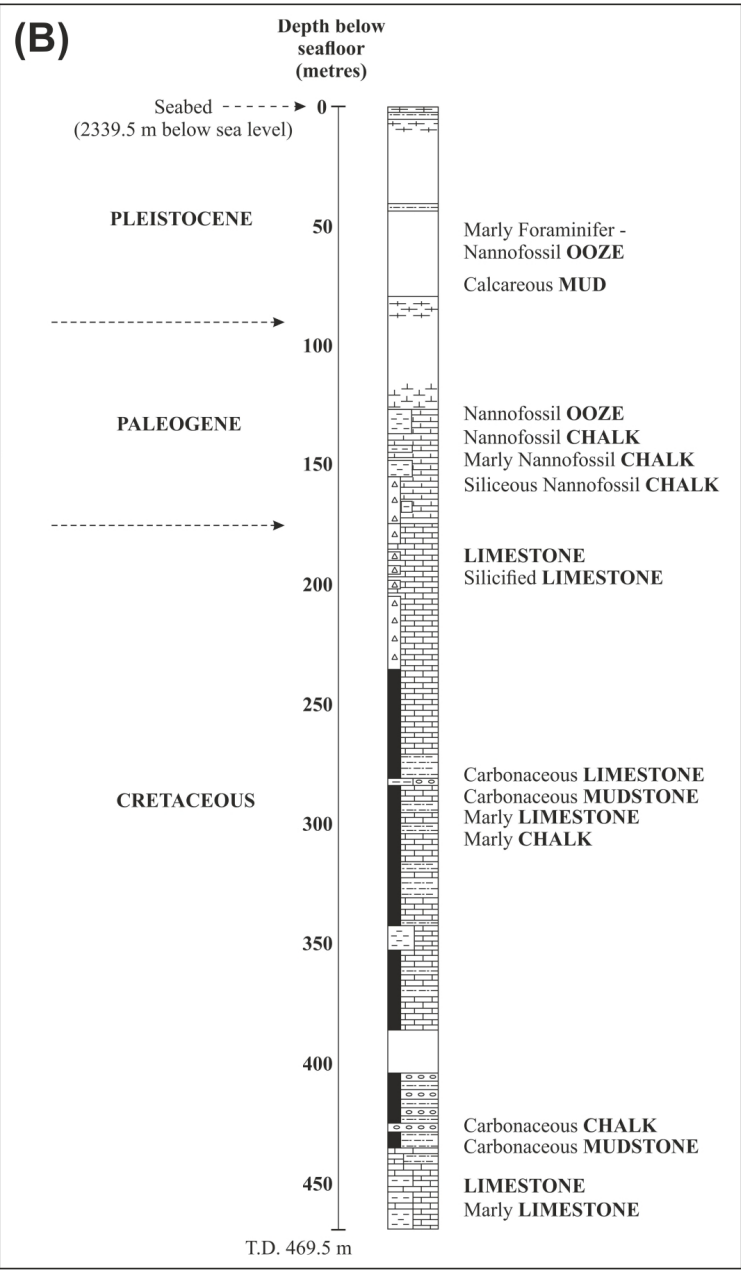
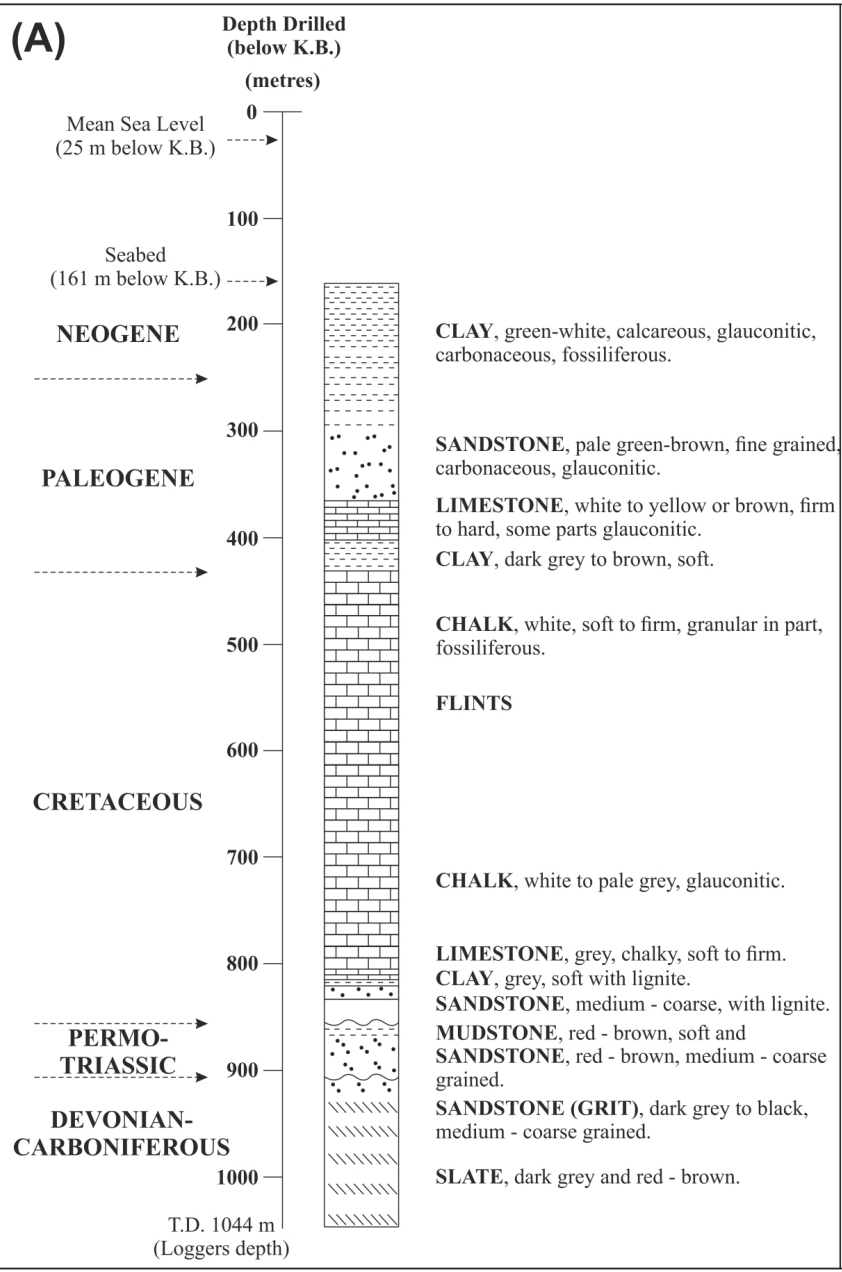
**Table 2: Point Load Index (PLI) testing results, showing the difference in strength values between pure and muddy carbonate samples.**

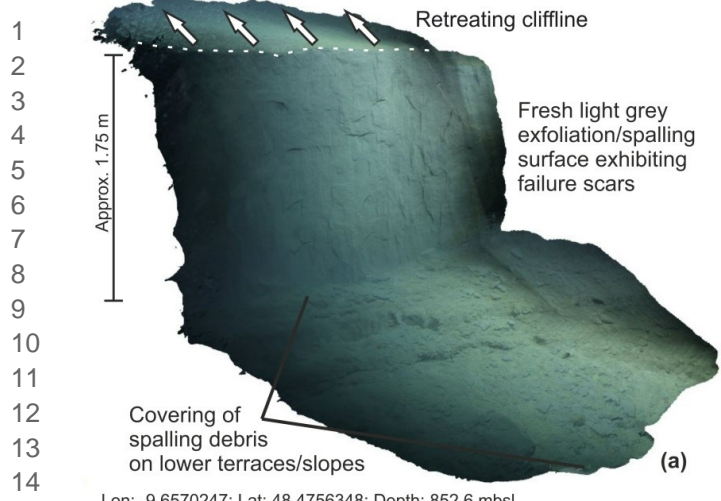
676  
 677  
 678

1  
2  
3  
4  
5  
6  
7  
8  
9  
10  
11  
12  
13  
14  
15  
16  
17  
18  
19  
20  
21  
22  
23  
24  
25  
26  
27  
28  
29  
30  
31  
32  
33  
34  
35  
36  
37  
38  
39  
40  
41  
42  
43  
44  
45  
46  
47  
48  
49  
50  
51  
52  
53  
54  
55  
56  
57  
58  
59  
60

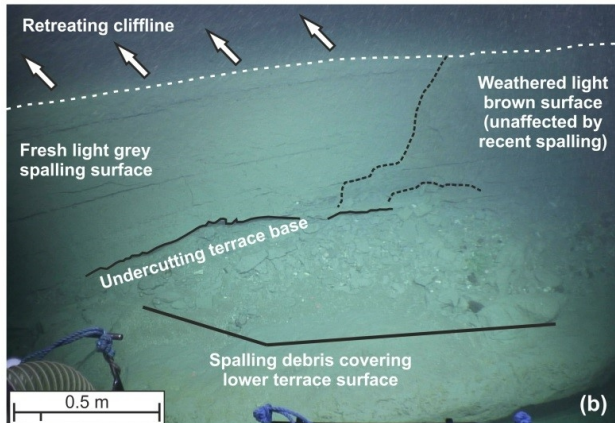


1  
2  
3  
4  
5  
6  
7  
8  
9  
10  
11  
12  
13  
14  
15  
16  
17  
18  
19  
20  
21  
22  
23  
24  
25  
26  
27  
28  
29  
30  
31  
32  
33  
34  
35  
36

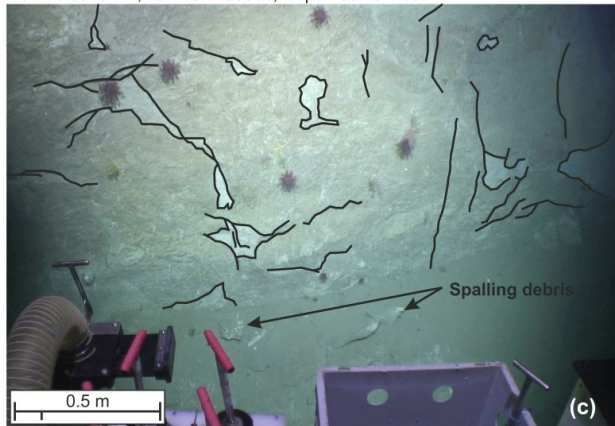




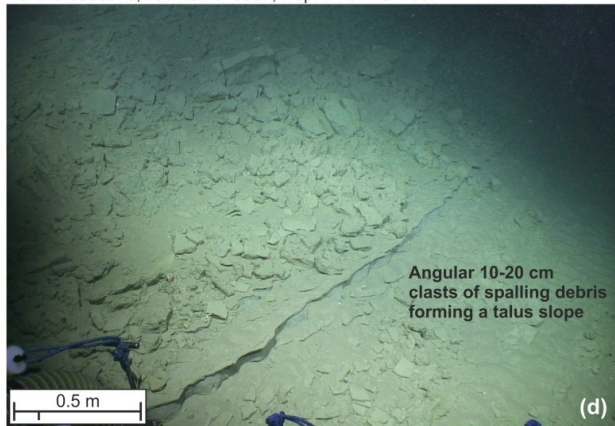
Lon: -9.6570247; Lat: 48.4756348; Depth: 852.6 mbsl



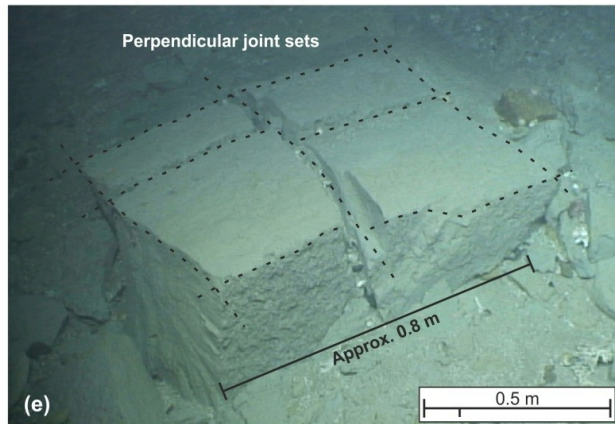
Lon: -9.6535018; Lat: 48.4675862; Depth: 1017.5 mbsl



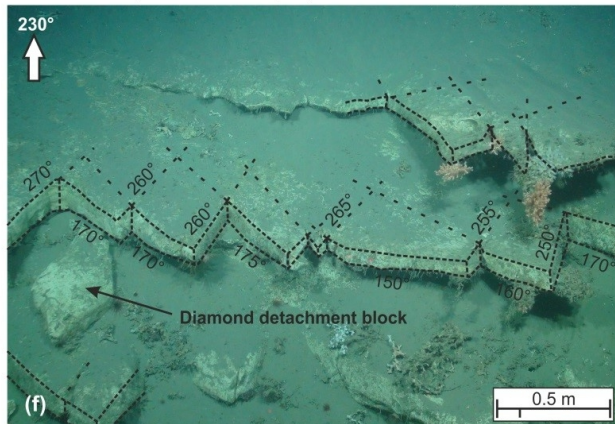
Lon: -11.199363; Lat: 48.6075657; Depth: 2617.1 mbsl



Lon: -9.6537852; Lat: 48.4693107; Depth: 1001.6 mbsl

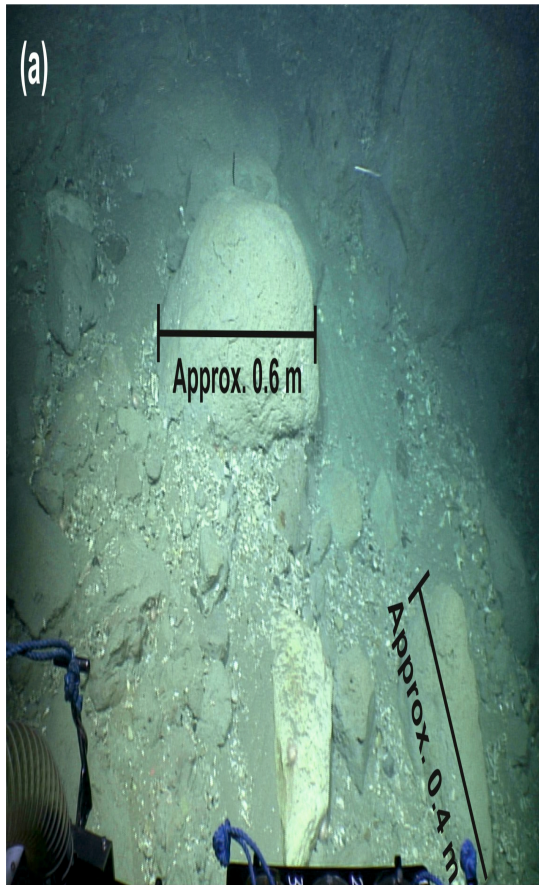


Lon: -9.6534137; Lat: 48.4674213; Depth: 1030.5 mbsl

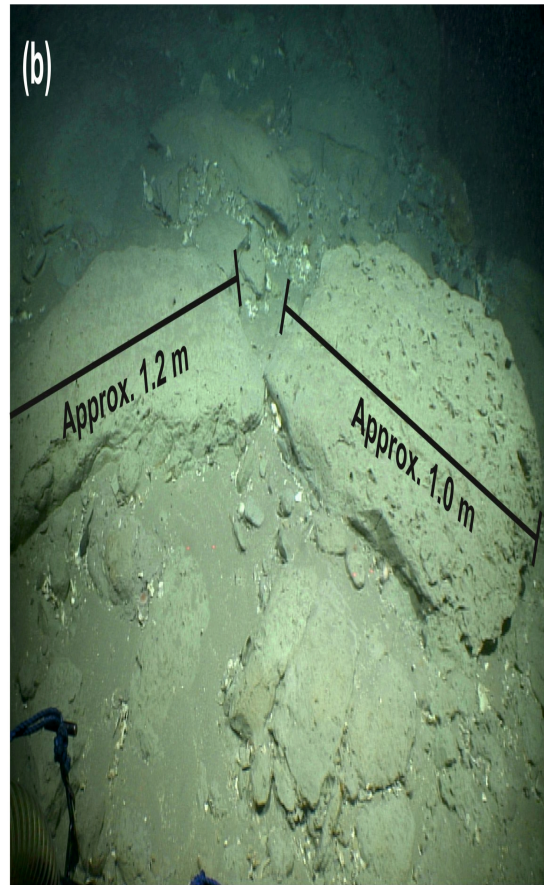


Lon: -10.4749982; Lat: 48.7530402; Depth: 740.0 mbsl

1  
2  
3  
4  
5  
6  
7  
8  
9  
10  
11  
12  
13  
14  
15  
16  
17  
18  
19  
20  
21  
22  
23  
24  
25  
26  
27  
28  
29  
30  
31  
32  
33  
34  
35  
36  
37  
38  
39  
40  
41  
42  
43  
44  
45  
46  
47  
48  
49  
50  
51  
52  
53  
54  
55  
56  
57  
58  
59  
60



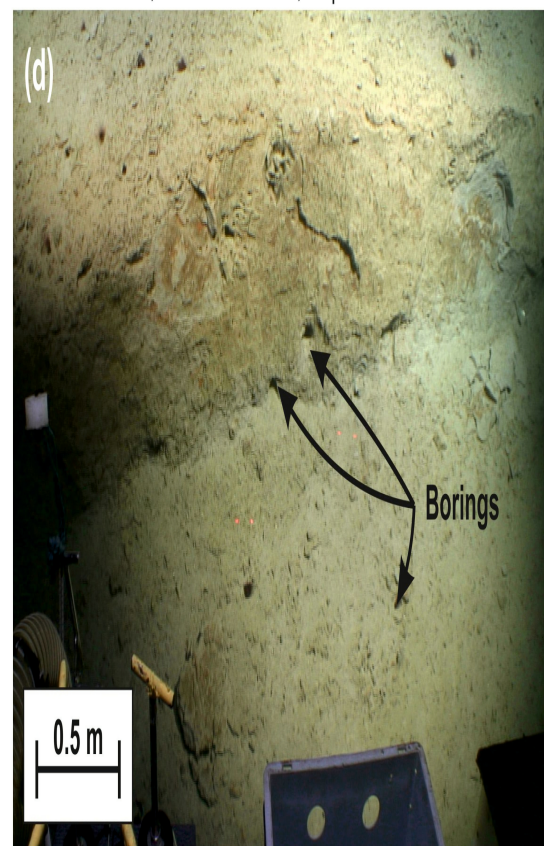
Lon: -9.6527113; Lat: 48.4660002; Depth: 1065.8 mbsl



Lon: -9.6527818; Lat: 48.4660627; Depth: 1064.8 mbsl



Lon: -9.639216; Lat: 48.465525; Depth: 736.2 mbsl



Lon: -9.6429888; Lat: 48.4673043; Depth: 864.2 mbsl



1  
2  
3  
4  
5  
6  
7  
8  
9  
10  
11  
12  
13  
14  
15  
16  
17  
18  
19  
20  
21  
22  
23  
24  
25  
26  
27  
28  
29  
30  
31  
32  
33  
34  
35  
36  
37  
38  
39  
40  
41  
42  
43  
44  
45  
46  
47  
48  
49  
50  
51  
52  
53  
54  
55  
56  
57  
58  
59  
60

